

Cite this: *Dalton Trans.*, 2024, **53**, 16879

Copper complexation of rosarin: formation of bis-copper rosarin and mono-copper linear tridipyrin complexes†

Xiaojuan Lv,^a Long Qian,^a Nikolay V. Tkachenko,^{*b,c} Tao Zhang,^{id a} Fengxian Qiu,^{id *a} Naoki Aratani,^{id *d} Takahisa Ikeue,^e Jianming Pan^a and Songlin Xue^{id *a}

A novel rosarin di-Cu complex **2Cu-1** and a linear six-pyrrolic mono-copper complex **1Cu-1** were synthesized using rosarin as the ligand. The molecular conformations of these complexes were confirmed by X-ray crystallography. The optical study of **1Cu-1** indicated NIR-II absorption due to the long six-pyrrolic ligand and the ICT effect. The **2Cu-1** complex exhibited a very narrow electronic reduction–oxidation gap of 0.50 eV, attributed to the antiaromatic characteristics of the rosarin ring. The first HER study of the di-copper rosarin complex **2Cu-1** indicated that the multi-metal poly-pyrrolic complexes are promising molecular hydrogen evolution reaction catalysts.

Received 29th July 2024,
Accepted 26th September 2024

DOI: 10.1039/d4dt02161d

rsc.li/dalton

Introduction

Poly-pyrrolic macrocycle molecules are native ligands that are used to form multi-metal complexes.^{1,2} Among these, hexaphyrins, typical expanded porphyrinoids that comprise six pyrrole rings, are significant owing to their various structures (planar topology and flexible topologies including figure-of-eight, Hückel and Möbius conformations),³ NIR absorption,⁴ diverse coordination abilities,^{3,4} multi-electron donation and withdrawing abilities.⁵ Since Dolphin's group reported the first *meso*-hexaphyrin(1.1.1.1.1.1) in 1997,⁶ the study of these macrocycles has expanded significantly. Copper is an attractive catalytic element that provides rich yields in various applications, including organic synthesis⁷ and photo/electrocatalytic reactions involving H₂O, O₂, N₂, and CO₂.⁸ As a consequence, copper porphyrinoid complexes have been extensively studied and are still attracting our attention, especially multi-

copper complexes since they are potential platforms for electron spin and synergistic catalysis between di-metal ions.^{5–9}

In 2004, Osuka's group reported a series of *meso*-hexaphyrin(1.1.1.1.1.1) dicopper complexes (Fig. 1). The copper coordination in these complexes cleaves the global aromatic ring of *meso*-hexaphyrin(1.1.1.1.1.1), with O and Cl atoms serving as linked bridges between di-copper ions.^{9a} In 1996 and 2007, Lynch and Sessler reported two di-copper complexes of hexaphyrin(1.0.0.1.0.0) and hexaphyrin(1.0.1.0.0.0), which are regarded as ring contracted hexaphyrins compared to hexaphyrin(1.1.1.1.1.1) (Fig. 1). These two di-copper complexes retained the global aromatic properties of their respective hexaphyrins, with di-copper sharing two Cl atoms as linked bridges.^{9b} In 2019, we reported a novel figure-of-eight shaped

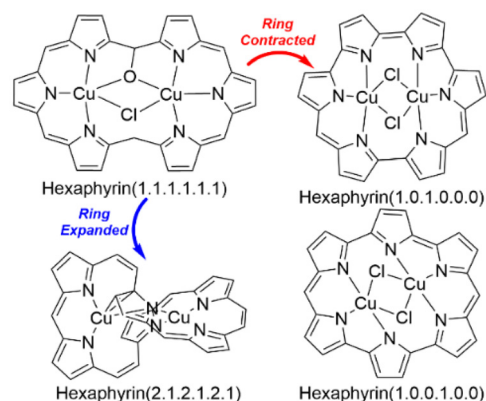


Fig. 1 Di-copper hexaphyrin complexes.

^aSchool of Chemistry and Chemical Engineering, Jiangsu University, 301 Xuefu Road, Zhenjiang 212013, China. E-mail: fxqiu@ujs.edu.cn, slxue@ujs.edu.cn

^bDepartment of Chemistry, University of California, Berkeley, CA 94720, USA

^cMaterials Sciences Division, Lawrence Berkeley National Laboratory, Berkeley, CA 94720, USA. E-mail: nikolaytkachenko@berkeley.edu

^dDivision of Materials Science, Nara Institute of Science and Technology, 8916-5 Takayama-cho, Nara 630-0192, Japan. E-mail: aratani@ms.naist.jp

^eDepartment of Materials Chemistry, Graduate School of Natural Science and Technology Shimane University, 1060 Nishikawatsu, Matsue, Shimane 690-8504, Japan

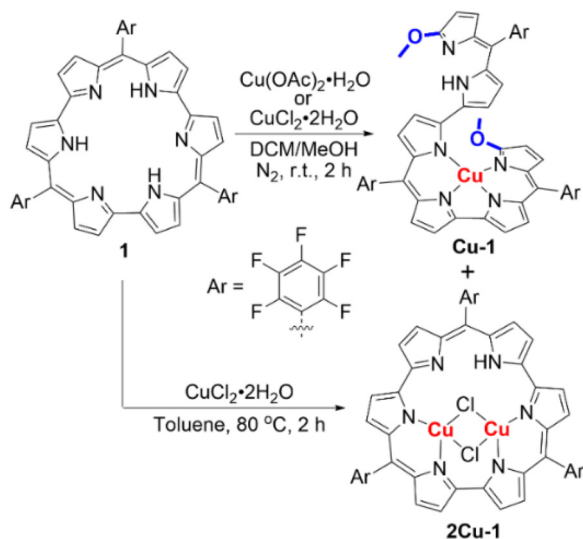
†Electronic supplementary information (ESI) available: Instrumentation and materials, detailed synthesis, theoretical calculations, supporting figures, and crystal data. CCDC 2365116 and 2365126. For ESI and crystallographic data in CIF or other electronic format see DOI: <https://doi.org/10.1039/d4dt02161d>

dicopper hexaphyrin(2.1.2.1.2.1) complex. Due to the flexible structure of hexaphyrin(2.1.2.1.2.1), copper ions can control the aromaticity and *cis/trans*-isomerization of hexaphyrin(2.1.2.1.2.1).⁵ Over the past years, we have been studying expanded porphyrins extensively.¹⁰ In 2022, we first reported highly planar hexaphyrin(1.0.1.0.1.0) (rosarin).¹¹ We found that it can form mono-Re,¹² di-Rh,^{4b} tri-Rh,^{4b} mono-B,¹³ and hybrid di-Rh/B¹³ complexes. These reported complexes of rosarin showed special and interesting properties, such as a highly stable antiaromatic ring,¹¹ stabilization of the neutral radical through hetero-bimetal coordination,¹³ and conflicting aromaticity in trirhodium(i) rosarin.^{4b}

In this work, we report a novel rosarin di-Cu complex (**2Cu-1**) and a linear six-pyrrolic copper complex (**Cu-1**) synthesized through a copper coordination reaction between antiaromatic rosarin (**1**) and copper salts. The molecular structures, optical and electronic properties, and chemical bonding of **Cu-1** and **2Cu-1** were investigated using high resolution mass spectrometry (HR-MS), electron paramagnetic resonance (EPR) spectroscopy, nuclear magnetic resonance (NMR) spectroscopy, X-ray crystallography, UV-Vis absorption, electrochemistry and theoretical calculations. Furthermore, due to the presence of two Cu ions, the hydrogen evolution reaction (HER) ability of **2Cu-1** was evaluated.

Results and discussion

The mono- and di-copper complexes of **1** were synthesized under two sets of coordination reaction conditions (Scheme 1). The rosarin **1** was reacted with 10 equivalents of $\text{CuCl}_2 \cdot 2\text{H}_2\text{O}$ or $\text{Cu}(\text{OAc})_2 \cdot \text{H}_2\text{O}$ in a dichloromethane (CH_2Cl_2)/MeOH mixture at room temperature under a N_2 atmosphere. Through purification by silica gel column chromatography, **Cu-1** and **2Cu-1** were isolated with yields of 6% and 48%, respectively.



Scheme 1 Syntheses of **Cu-1** and **2Cu-1**.

High-resolution mass spectrometry (HR-MS) and X-ray diffraction of **Cu-1** revealed that it is a linear six-pyrrolic copper complex. Due to the presence of $-\text{MeO}$ groups that cut the macrocyclic ring, toluene was chosen as a solvent to facilitate coordination at high temperatures. The rosarin **1** was reacted with 10 equivalents of $\text{CuCl}_2 \cdot 2\text{H}_2\text{O}$ in toluene at 80°C under a N_2 atmosphere for 2 h. Under these conditions, only **2Cu-1** was isolated in 64% yield. The HR-MS spectra of **Cu-1** and **2Cu-1** exhibit the corresponding molecular ion peaks at $m/z = 1047.0606$ $[\text{M}]^+$ (calcd for $\text{C}_{47}\text{H}_{19}\text{CuF}_{15}\text{N}_6\text{O}_2 = 1047.0626$ $[\text{M}]^+$) and $m/z = 1118.9015$ $[\text{M} + \text{H}]^+$ (calcd for $\text{C}_{45}\text{H}_{13}\text{Cl}_2\text{Cu}_2\text{F}_{15}\text{N}_6 = 1117.8931$ $[\text{M}]^+$), respectively (Fig. S1 and S2, ESI[†]). The EDS elemental experiments showed the presence of C, F, N, Cu and Cl elements in the **2Cu-1** complex (Fig. S3, ESI[†]).

Suitable single crystals of **Cu-1** and **2Cu-1** were grown by slow evaporation of CH_2Cl_2 solution (Fig. 2 and crystal data in the ESI[†]). In **Cu-1**, the macrocyclic antiaromatic ring was cut by two $-\text{MeO}$ groups of **1** to form a linear structure.¹⁴ Two of the three dipyrin units in **Cu-1** are coordinated with one copper ion, while the third dipyrin unit remains uncoordinated (Fig. 2a). The copper(II) ion of **Cu-1** is coordinated to four nitrogen atoms of two dipyrin units in a distorted square planar geometry. The angle between the coordinated two dipyrin units is 25.5° . The single crystal of **2Cu-1** exhibits a disorder involving three copper positions (Fig. 2 and crystal data in the ESI[†]). The free-base **1** exhibited good planarity,¹¹ whereas the main rosarin skeleton of **2Cu-1** is slightly distorted. The mean plane deviation (MPD, defined by the 33 core C and N atoms) of **2Cu-1** reaches 0.23 \AA . **2Cu-1** has a significant bond-length alternation, which is consistent with the antiaromatic nature of rosarin.¹¹ The bond-length differences between neighbouring $\text{C}_{\text{meso}}-\text{C}_\alpha$ bonds in **2Cu-1** are 0.050 , 0.033 , and 0.047 \AA (Fig. 2b). Furthermore, the Cu–Cu distance in **2Cu-1** is longer than the typical Cu–Cu bond in the Cu_2 dimer (2.26 \AA), indicating weak or no interaction between copper ions in **2Cu-1**.¹⁵

An attempt was made to record the ^1H NMR spectrum for **2Cu-1**. The spectrum revealed two very broad peaks corresponding to β -pyrrolic H-atoms, indicating the open-shell structure of **2Cu-1** (Fig. S4, ESI[†]). Thus, EPR analysis is required to reveal the nature and features of the **2Cu-1** open-shell system

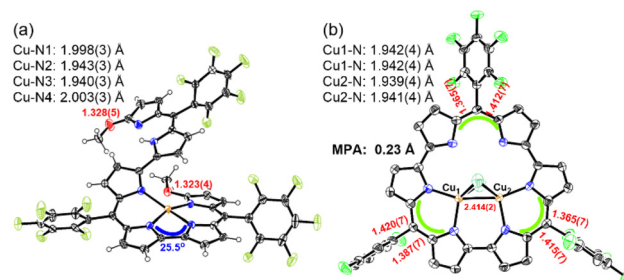


Fig. 2 Single crystal structures of (a) **Cu-1** and (b) **2Cu-1** with selected bond distances (Å). Thermal ellipsoids are shown at 40% probability. The hydrogen atoms and disordered parts of **2Cu-1** are omitted for clarity.

(Fig. S5, ESI†). Given the even number of electrons, we expect that at least two unpaired electrons are present in the structure. The EPR spectrum of **2Cu-1** exhibited g values of 2.08 and 2.29. The observed EPR spectrum is in good agreement with the simulated spectrum with the spin Hamiltonian parameters: $S = 1$, $g_{\perp} = 2.08$, $g_{\parallel} = 2.29$, $D = 5.01 \times 10^{-3} \text{ cm}^{-1}$, $E = 1.67 \times 10^{-3} \text{ cm}^{-1}$, $A_{\perp}(\text{Cu}) = 5.00 \times 10^{-4} \text{ cm}^{-1}$, $A_{\parallel}(\text{Cu}) = 8.00 \times 10^{-3} \text{ cm}^{-1}$, $A_{\perp}(\text{N}) = 3.50 \times 10^{-3} \text{ cm}^{-1}$, and $A_{\parallel}(\text{N}) = 2.00 \times 10^{-3} \text{ cm}^{-1}$.¹⁶ This simulated result indicates that the two unpaired electrons effectively exhibit zero coupling between each other.¹⁷

To reveal the nature of Cu–Cu interactions within **2Cu-1** and analyze its spin density distribution, we performed hybrid DFT analysis of the synthesized complex. Geometries for different spin states (singlet, triplet, and quintet) were optimized to reveal the energetically lowest spin state. Upon optimization, the geometries for different spin states were found to be mainly similar, retaining the main structural features. The calculated Cu–Cu distances for singlet, triplet, and quintet states are 2.36 Å, 2.34 Å, and 2.86 Å, respectively. The most energetically stable spin state was found to be the triplet state, which is lower in energy by 25.4 kcal mol⁻¹ compared to the closed-shell singlet state and 20.5 kcal mol⁻¹ compared to the open-shell quintet state. The computed Cu–Cu distance for the ground triplet state is slightly shorter than the experimentally obtained Cu–Cu distance for **2Cu-1**, which can be attributed to the underestimation of the metal–metal bond distance with hybrid functionals. Further optimization of the structure using the GGA PBE method resulted in a Cu–Cu distance of 2.41 Å, which shows better agreement with the experimental values.

The unpaired spin density for the optimized triplet structure is shown in Fig. 3a. As observed, the spin density is significantly delocalized with the major density spreading to the rosarin ligand and Cu₂ parts. By integrating the spin densities, it is evident that approximately one electron is localized on the Cu₂ fragment, while the other electron resides on the rosarin part. Similar spin density delocalization was observed before in copper-containing compounds.¹⁷ In the geometry of triplet species, we also calculated the broken-symmetry open-shell singlet to understand the spin-coupling constant between two unpaired electrons. The calculated spin-coupling constant was found to be close to 0 eV, which agrees with the EPR results.

Because the Cu–Cu distance of **2Cu-1** is longer than a typical Cu–Cu bond,¹⁵ we decided to decipher the chemical bonding pattern of **2Cu-1** using the Adaptive Natural Density Partitioning (AdNDP) localization scheme. The AdNDP and NBO analyses revealed four lone pairs on each Cl atom, formally giving them a charge of -1. Additionally, five alpha d-type electrons and four beta d-type electrons were localized on each Cu atom. However, beta electron density partitioning reveals the presence of an additional 2c-1e Cu–Cu σ -bond with an occupation number of 0.99|e|, formed by d-orbitals (Fig. 3b). This gives the Cu₂ fragment a +3 formal charge (since there are 19 valence electrons on two Cu atoms, while a neutral Cu₂ would have 22 electrons) and a formal average oxidation state of +1.5 for each Cu atom. This chemical bonding

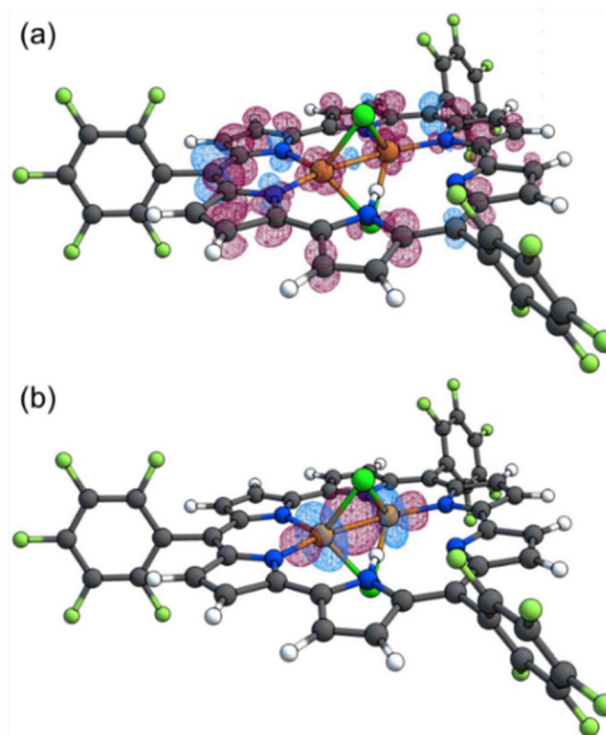


Fig. 3 (a) Spin density map of **2Cu-1** obtained at the CAM-B3LYP-D3 (BJ)/def2-SVP level of theory; and (b) the 2c-1e Cu–Cu σ -bond element and its occupation number obtained from the AdNDP analysis of **2Cu-1**.

analysis is consistent with the observed spin-density distribution, where the Cu₂ fragment has one unpaired electron (from AdNDP we have 10 alpha and 9 beta electrons on the Cu₂ fragment). The rest of the chemical bonding is in agreement with the AdNDP analysis of previously studied rosarin complexes,^{4b} with the only difference being that instead of having six delocalized 33c-2e bonds on the rosarin ligand, we have five delocalized 33c-2e bonds and the presence of an unpaired 33c-1e bond with an occupation number of 0.98|e|. The presence of 11 instead of 12 delocalized electrons in the rosarin ring makes its antiaromatic characteristics less pronounced. The QTAIM analysis confirms the presence of weak interactions between Cu atoms, revealing a bond critical point between Cu atoms with a low electron density of 0.05 a.u. and an electron localization function (ELF) value of 0.25, indicating the presence of weak bonding interactions.

The optical properties of **Cu-1** and **2Cu-1** were investigated using UV-vis-NIR absorption spectra in CH₂Cl₂ (Fig. S6a, ESI†). The **2Cu-1** complex exhibited a main absorption band at 484 nm. Interestingly, the linear six-pyrrolic complex **Cu-1** exhibited a main absorption band at 537 nm and other bands in the NIR region, at 830 and 930 nm. These absorption spectra reflect the antiaromaticity of **2Cu-1** and the open-chain tetrapyrrolic metal complex of **Cu-1**.^{11,12,18} The TD-DFT analysis of **1Cu-1** was performed to evaluate the optical absorption. The ICT of the band at 930 nm was confirmed (Fig. S7 and S8 and Table S1, ESI†).¹⁹ The redox properties of **2Cu-1**

were measured using cyclic voltammetry (CV) and differential pulse voltammetry (DPV) in CH_2Cl_2 (Fig. S6b, ESI†). The amount of **Cu-1** is too small to perform CV and DPV. **2Cu-1** showed three reversible oxidation and two reversible reduction $E_{1/2}$ potentials at 0.84, 0.43, 0.17, -0.33 , and -0.56 V (vs. SCE). The cyclic voltammetry results of **2Cu-1** show that the first oxidation (E_{ox1}) and first reduction (E_{red1}) $E_{1/2}$ potentials gave a very narrow gap of 0.50 eV ($E_{\text{gap, cv}} = E_{\text{ox1}} - E_{\text{red1}}$).^{10–12} Based on our previous work,^{11–13} these oxidation–reduction peaks are attributed to the macrocycle itself. The DFT calculated SOMO (α)–SUMO(β) gaps of **2Cu-1** are 1.44 and 1.65 eV, respectively (Fig. S9, ESI†). The relatively narrow calculated SOMO(α)–SUMO(β) gaps are due to the antiaromatic rosarin ring.^{1,3,11}

The **2Cu-1** was loaded on a carbon nanotube (CNT) to obtain the HER ink **2Cu-1@CNT** to investigate its heterogeneous electrocatalytic HER capacity in 0.5 M H_2SO_4 aqueous solutions at room temperature.^{10c} The HER ink morphology of **2Cu-1@CNT** was characterised by using scanning electron microscopy (SEM) and mapping images (Fig. S10, ESI†), which showed uniform distribution of **2Cu-1** on the CNT. The typical Cu signals of **2Cu-1@CNT** were confirmed by X-ray photoelectron spectroscopy (XPS) (Fig. S11, ESI†). The high-resolution XPS spectra of Cu $2p_{1/2}$ and Cu $2p_{3/2}$ showed peaks at 936.1 and 953.2 eV, respectively, corresponding to Cu ions, which is similar to the XPS result of the porphyrin(1.1.1.1) Cu complex and the benzene-fused porphyrin(2.1.2.1) complex loaded on CNTs.^{10c} The SEM and XPS results indicated that we successfully prepared the HER ink. The linear sweep voltammograms (LSVs) of **2Cu-1@CNT** show that it was more HER active in aqueous solutions (Fig. 4a). **2Cu-1@CNT** gave a lower overpotential (550 mV) than the porphyrin(2.1.2.1) copper, benzene-fused porphyrin(2.1.2.1) di-copper and porphyrin(1.1.1.1) copper complexes to actuate a current density of 10 mA cm^{-2} under the same HER measurement conditions.^{10c,20} The LSV result of **2Cu-1@CNT** is evidence that **2Cu-1** is a good di-copper porphyrinoid heterogeneous HER

catalyst.^{10c,20} The ideal HER activity of **2Cu-1** is due to di-Cu ions and strong π – π interactions between the rosarin larger π -ligand of **2Cu-1** and the CNT.^{10c,21} The Tafel plot of **2Cu-1@CNT** is 190 mV dec^{-1} (Fig. 4b). The Nyquist plot of **2Cu-1@CNT** has a semicircular shape, and the diameter of the semicircular is smaller than that of copper porphyrinoid heterogeneous HER catalysts, indicating that **2Cu-1@CNT** has a lower charge transfer resistance (R_{ct}) (Fig. 4c). CV was conducted at different scan rates (Fig. 4d) to estimate the electrochemically active surface area (ECSA) by measuring C_{dl} (Fig. S12, ESI†). The C_{dl} value of **2Cu-1@CNT** is 1.5 mF cm^{-2} , indicating that **2Cu-1@CNT** exhibits high HER catalytic activity as a molecular catalyst. The HER catalytic stability of **2Cu-1@CNT** was demonstrated using an I – t test (Fig. S13, ESI†). **2Cu-1@CNT** was shown to be stable during electrolysis in 0.5 M H_2SO_4 for the HER for 12 000 s. The stability of **2Cu-1** after the HER catalysis was also investigated by UV-Vis spectroscopy. After catalysis, **2Cu-1** was obtained using ultrasound at the electrode. The absorption spectrum of **2Cu-1** after HER catalysis supports the good stability of **2Cu-1** (Fig. S14, ESI†). The first HER study attempt of the di-copper hexaphyrin complex indicated that the multi-metal ploy-pyrrolic complexes are promising molecular HER catalysts.

Experimental

Instrumentation and materials

The UV-vis absorption spectra were recorded with a JASCO UV/VIS/NIR spectrophotometer V-670. The ^1H NMR spectrum was recorded on a JNM-ECX 400 spectrometer (operating at 400 MHz for ^1H) using the residual solvent as the internal reference for ^1H ($\delta = 7.26$ ppm in CDCl_3). The APCI-FT-MS mass spectrum was recorded on a Thermo Fisher Scientific spectrometer. All solvents and chemicals were used without further purification except as noted. The HR-MALDI-TOF-MS spectrum was recorded on a Bruker Daltonics autoflex MALDI-TOF-MS spectrometer. The electron paramagnetic resonance spectroscopy (EPR) signal of the copper complex was measured using a Bruker EMXplus spectrometer. X-ray crystallographic data for CCDC: 2365116 (**Cu-1**) were recorded at 193 K on a Bruker D8 VENTURE TXS PHOTON 100 diffractometer using $\text{MoK}\alpha$ radiation from the corresponding set of confocal optics. X-ray crystallographic data for CCDC: 2365126 (**2Cu-1**) were recorded at 193 K on a Bruker APEX-II CCD diffractometer using $\text{GaK}\alpha$ radiation from the corresponding set of confocal optics. They both used Olex2,²² and the structures were solved with the SHELXT²³ structure solution program using intrinsic phasing and refined with the SHELXL²⁴ refinement package using least squares minimization. Cyclic voltammetry (CV) and differential pulse voltammetry (DPV) were conducted in a solution of 0.1 M TBAP in CH_2Cl_2 at a scan rate of 0.1 V s^{-1} in an N_2 -filled cell. A glassy carbon electrode and a platinum wire were used as a working and a counter electrode, respectively. A saturated calomel electrode (SCE) was used as a

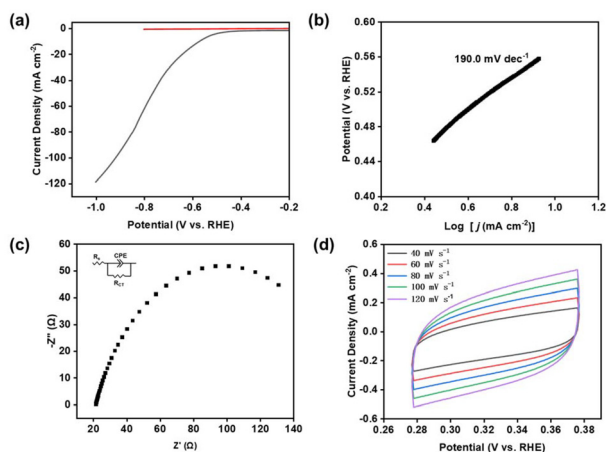


Fig. 4 (a) Blank LSV curves (red line) and HER LSV curves (black line) of **2Cu-1** in 0.5 M H_2SO_4 , (b) Tafel slope plot, (c) Nyquist plot and (d) CVs at different scan rates of **2Cu-1@CNT**.

reference electrode. All density functional theory calculations were performed with the Gaussian 16 program package.²⁵

Electrochemical study

The linear sweep voltammograms (LSVs) were acquired in 0.50 M H₂SO₄ using a three-compartment cell with a glassy carbon working electrode, a graphite rod auxiliary electrode, and an Ag/AgCl (saturated with KCl) reference electrode. The preparation of the catalyst-coated glassy carbon electrode is described as follows. To 1.0 mL of freshly distilled acetonitrile, 1.0 mg of CNTs, 1.0 mg of **2Cu-1**, and 25 μ L of Nafion (5.0 wt%, DuPont) were added. The resultant mixture was sonicated using an ultrasonic cleaner for 30 min to obtain an ink. Then, 4 μ L of the suspension was added dropwise onto the surface of a freshly polished glassy carbon electrode. After drying at room temperature, the prepared glassy carbon electrodes were used for electrochemical studies. The 0.50 M H₂SO₄ aqueous solution was bubbled with N₂ for 30 min before analysis. The electrolysis of **2Cu-1**@CNT was performed with a three-electrode H-type cell containing a Nafion membrane (Nafion@117, DuPont, Inc.) to separate the carbon paper working electrode (0.5 cm², loading with catalysts) and the other two electrodes.

General synthesis

Conditions A. A solution of **1** (27.8 mg, 0.03 mmol) and 10 equiv. of CuCl₂·2H₂O or Cu(OAc)₂·2H₂O (0.3 mmol) in a CH₂Cl₂/MeOH mixture (5/1, 30 ml) was stirred at room temperature for 2 h under a N₂ atmosphere. After removal of the reaction solvent, the crude solid was purified by silica gel column chromatography (CH₂Cl₂/hexane = 1/3) to obtain **Cu-1** and **2Cu-1** in yields of 6% (1.9 mg, 0.0018 mmol) and 48% (16.1 mg, 0.0144 mmol), respectively. Both copper complexes are black solids.

Conditions B. A solution of **1** (27.8 mg, 0.03 mmol) and 10 equiv. of CuCl₂·2H₂O (0.3 mmol) in toluene was stirred at 80 °C for 2 h under a N₂ atmosphere. After removal of the reaction solvent, the crude solid was purified by silica gel column chromatography (CH₂Cl₂/hexane = 1/3) to form only **2Cu-1** in 64% yield (21.5 mg, 0.0192 mmol).

Cu-1. HR-APCI-MS: $m/z = 1047.0606 [M]^+$ (calcd for C₄₇H₁₉CuF₁₅N₆O₂ = 1047.0626 [M]⁺). UV-Vis-NIR (in CH₂Cl₂) λ [nm] (ϵ [M⁻¹ cm⁻¹]): 537 (188 000), 830 (33 000), 930 (38 000) nm.

2Cu-1. HR-MALDI-MS: $m/z = 1118.9015 [M + H]^+$ (calcd for C₄₅H₁₃Cl₂Cu₂F₁₅N₆ = 1117.8931 [M]⁺). UV-Vis-NIR (in CH₂Cl₂) λ [nm] (ϵ [M⁻¹ cm⁻¹]): 484 (132 000) nm.

Computational methods of Cu–Cu interactions

The geometries of **2Cu-1** at different spin states were optimized using the Gaussian 16 program package.²⁵ A range-separated CAM-B3LYP hybrid functional²⁶ with D3 Grimme's dispersion correction with Beck–Johnson damping (D3(BJ))²⁷ was employed. Additionally, the GGA PBE functional²⁸ was used to optimize the ground triplet state geometry to obtain more accurate Cu–Cu distances. For the optimization procedure,

chemical bonding analysis, and Hessian calculations, a well-balanced DZ basis (def2-SVP) was utilized.²⁹ Chemical bonding analysis was performed using Multiwfn,³⁰ NBO³¹ and AdNDP 2.0³² software. Spin coupling constant calculations were carried out using ORCA 5.0.4 software.³³

Conclusions

We synthesized di-copper rosarin and mono-copper linear tri-dipyrrin complexes from rosarin as the ligand. X-ray crystallography confirmed the mono-copper linear tridipyrrin structure of **Cu-1** and the bis-copper rosarin conformation of **2Cu-1**. EPR and theoretical calculations revealed the presence of weak bonding interactions between Cu and Cu within **2Cu-1**. The optical study of **Cu-1** indicated its NIR-II absorption due to the long six-pyrrolic ligand and the ICT effect. The CV of **2Cu-1** exhibited a very narrow $E_{\text{gap, cv}} = E_{\text{ox1}} - E_{\text{red1}}$ gap. The first HER study of the di-copper rosarin complex **2Cu-1** was performed, and the HER capacity of **2Cu-1** indicates that the multi-metal ploy-pyrrolic complexes are promising molecular HER catalysts.

Data availability

The data that support the findings of this study are available from the corresponding author, sxue@ujs.edu.cn (Prof. Dr Songlin Xue), upon reasonable request.

Conflicts of interest

There are no conflicts to declare.

Acknowledgements

This work in China was supported by the National Natural Science Foundation of China (22301108). The work at NAIST was partly supported by Grants-in-Aid for Scientific Research (No. JP23K26480 and JP23H01787).

References

- 1 T. Tanaka and A. Osuka, *Chem. Rev.*, 2017, **117**, 2584.
- 2 A. Majeed, L. Mohammed, O. Hammoodi, S. Sehgal, M. Alheety, K. Saxena, S. Dadoosh, I. Mohammed, M. Jasim and N. Salmaan, *Int. J. Polym. Sci.*, 2022, 9047554.
- 3 (a) J. L. Sessler and D. Seidel, *Angew. Chem., Int. Ed.*, 2003, **42**, 5134; (b) Z. S. Yoon, A. Osuka and D. Kim, *Nat. Chem.*, 2009, **1**, 113; (c) M. Stepien, N. Sprutta and L. Latos-Grazynski, *Angew. Chem., Int. Ed.*, 2011, **50**, 4288; (d) A. Osuka and S. Saito, *Chem. Commun.*, 2011, **47**, 4330.
- 4 (a) S. Sahoo, M. Janaa and H. Rath, *Chem. Commun.*, 2022, **58**, 1834; (b) S. Xue, N. Tkachenko, F. Wu, X. Lv, N. Liu,

- A. Muñoz-Castro, S. Ueno, K. Matsuo, D. Kuzuhara, N. Aratani, Z. Shen, H. Yamada, A. Boldyrev and F. Qiu, *Inorg. Chem.*, 2024, **63**, 11494.
- 5 S. Xue, D. Kuzuhara, N. Aratani and H. Yamada, *Angew. Chem., Int. Ed.*, 2019, **58**, 12524.
- 6 C. Bruckner, E. D. Sternberg, R. W. Boyle and D. Dolphin, *Chem. Commun.*, 1997, **17**, 1689.
- 7 (a) X. Liu and Y. Huang, *Coord. Chem. Rev.*, 2023, **489**, 215173; (b) R. Zhang, Y. Chen, M. Ding and J. Zhao, *Nano Res.*, 2021, **15**, 2810.
- 8 (a) H. Kale, A. Kute, R. Gaikwad, P. Fornasiero, R. Zbořil and M. Gawande, *Coord. Chem. Rev.*, 2024, **502**, 215602; (b) B. Li, Y. Zhu and W. Guo, *Inorg. Chem. Front.*, 2023, **10**, 5812; (c) F. Chang, M. Xiao, R. Miao, Y. Liu, M. Ren, Z. Jia, D. Han, Y. Yuan, Z. Bai and L. Yang, *Electrochem. Energy Rev.*, 2022, **5**, 4.
- 9 (a) S. Shimizu, V. Anand, R. Taniguchi, K. Furukawa, T. Kato, T. Yokoyama and A. Osuka, *J. Am. Chem. Soc.*, 2004, **126**, 12280; (b) L. Jonathan, J. Sessler, J. Patricia, P. Melfi, E. Elisa Tomat, M. Vincent and V. Lynch, *Dalton Trans.*, 2007, 629; (c) H. Mori and A. Osuka, *Chem. – Eur. J.*, 2015, **21**, 7007; (d) Q. Chen, N. Fridman, B. Tumanskii and Z. Gross, *Chem. Sci.*, 2021, **12**, 12445.
- 10 (a) S. Xue, X. Lv, N. Liu, Q. Zhang, H. Lei, R. Cao and F. Qiu, *Inorg. Chem.*, 2023, **62**, 1679; (b) Y. Dong, X. Lv, Y. Sun, Q. Zhao, H. Lei, F. Wu, T. Zhang, Z. Xue, R. Cao, F. Qiu and S. Xue, *Inorg. Chem.*, 2024, **63**, 4797; (c) Y. Dong, L. Qian, F. Chen, Y. Wang, T. Zhang, F. Qiu, T. Teranishi and S. Xue, *Chem. Commun.*, 2024, **60**, 3986; (d) X. Lv, Y. Dong, J. Wu, T. Jiang, F. Chen, T. Zhang, F. Qiu and S. Xue, *Dalton Trans.*, 2024, **53**, 5979.
- 11 N. Liu, H. Morimoto, F. Wu, X. Lv, B. Xiao, D. Kuzuhara, J. Pan, F. Qiu, N. Aratani, Z. Shen, H. Yamada and S. Xue, *Org. Lett.*, 2022, **24**, 3609.
- 12 X. Lv, H. Gao, F. Wu, N. Liu, S. Ueno, X. Yang, T. Zhang, N. Aratani, H. Yamada, F. Qiu, Z. Shen and S. Xue, *Inorg. Chem.*, 2023, **62**, 4747.
- 13 S. Xue, Y. Dong, X. Lv, F. Qiu, Y. Wang, H. Furuta, T. Teranishi and F. Wu, *Chem. – Eur. J.*, 2024, **30**, e202400812.
- 14 Q. Li, C. Li, G. Baryshnikov, Y. Ding, C. Zhao, T. Gu, F. Sha, X. Liang, W. Zhu, X. Wu, H. Ågren, J. Sessler and Y. Xie, *Nat. Commun.*, 2020, **11**, 5289.
- 15 (a) C. Horn, I. Dance, D. Craig, M. Scudder and G. Bowmaker, *J. Am. Chem. Soc.*, 1998, **120**, 10549; (b) M. Bouammali, N. Suaud, N. Guihéry and R. R. mi Maurice, *Inorg. Chem.*, 2022, **61**, 12138; (c) I. Dutta, S. De, S. Yadav, R. Mondol and J. Bera, *J. Organomet. Chem.*, 2017, **849**, 117; (d) W. Taylor, U. Soto, V. Lynch and M. Rose, *Inorg. Chem.*, 2016, **55**, 3206.
- 16 S. Stoll and A. Schweiger, *J. Magn. Reson.*, 2006, **178**, 42.
- 17 K. Yamasumi, K. Nishimura, Y. Hisamune, Y. Nagae, T. Uchiyama, K. Kamitani, T. Hirai, M. Nishibori, S. Mori, S. Karasawa, T. Kato, K. Furukawa, M. Ishida and H. Furuta, *Chem. – Eur. J.*, 2017, **23**, 15322.
- 18 S. Larsen, J. Adewuyi, G. Ung and A. Ghosh, *Inorg. Chem.*, 2023, **62**, 7483.
- 19 L. Bucher, L. Tanguy, D. Fortin, N. Desbois, P. Harvey, G. Sharma and C. Gros, *ChemPlusChem*, 2017, **82**, 625.
- 20 X. Peng, J. Han, X. Li, G. Liu, Y. Xu, Y. Peng, S. Nie, W. Li, X. Li, Z. Chen, H. Peng, R. Cao and Y. Fang, *Chem. Commun.*, 2023, **59**, 10777.
- 21 (a) D. Khusnutdinova, B. Wadsworth, M. Flores, A. Beiler, E. Cruz, Y. Zenkov and G. Moore, *ACS Catal.*, 2018, **8**, 9888; (b) S. Chandra, A. Hazari, Q. Song, D. Hunger, N. Neuman, J. Slageren, E. Klemm and B. Sarkar, *ChemSusChem*, 2023, **16**, e202201146; (c) C. Ehli, A. Rahman, N. Jux, D. Balbinot, D. Guldi, F. Paolucci, M. Marcaccio, D. Paolucci, M. Melle-Franco, F. Zerbetto, S. Campidelli and M. Prato, *J. Am. Chem. Soc.*, 2006, **128**, 11222.
- 22 O. V. Dolomanov, L. J. Bourhis, R. J. Gildea, J. A. K. Howard and H. Puschmann, *J. Appl. Crystallogr.*, 2009, **42**, 339.
- 23 G. M. Sheldrick, *Acta Crystallogr.*, 2015, **71**, 3.
- 24 G. M. Sheldrick, *Acta Crystallogr.*, 2015, **71**, 3.
- 25 M. J. Frisch, G. W. Trucks, H. B. Schlegel, G. E. Scuseria, M. A. Robb, J. R. Cheeseman, G. Scalmani, V. Barone, G. A. Petersson, H. Nakatsuji, *et al.*, *Gaussian 16, Revision C.01*, Gaussian, Inc., Wallingford CT, 2019.
- 26 T. Yanai, D. P. Tew and N. C. Handy, *Chem. Phys. Lett.*, 2004, **393**, 51.
- 27 S. Grimme, S. Ehrlich and L. Goerigk, *J. Comput. Chem.*, 2022, **32**, 1456.
- 28 P. Perdew, K. Burke and M. Ernzerhof, *Phys. Rev. Lett.*, 1996, **77**, 3865.
- 29 F. Weigenda and R. Ahlrichs, *Phys. Chem. Chem. Phys.*, 2005, **7**, 3297.
- 30 T. Lu and F. Chen, *J. Comput. Chem.*, 2012, **33**, 580.
- 31 E. D. Glendening, J. K. Badenhoop, A. E. Reed, J. E. Carpenter, J. A. Bohmann, C. M. Morales, P. Karafiloglou, C. R. Landis and F. Weinhold, *NBO 7.0*, Theoretical Chemistry Institute, University of Wisconsin, Madison, 2018.
- 32 (a) D. Y. Zubarev and A. I. Boldyrev, *Phys. Chem. Chem. Phys.*, 2008, **10**, 5207; (b) N. V. Tkachenko and A. I. Boldyrev, *Phys. Chem. Chem. Phys.*, 2019, **21**, 9590; (c) N. V. Tkachenko, W.-X. Chen, H. W. T. Morgan, A. Muñoz-Castro, A. I. Boldyrev and Z.-M. Sun, *Chem. Commun.*, 2022, **58**, 6223; (d) H.-L. Xu, N. V. Tkachenko, Z.-C. Wang, W.-X. Chen, L. Qiao, A. Muñoz-Castro, A. I. Boldyrev and Z.-M. Sun, *Nat. Commun.*, 2020, **11**, 5286.
- 33 (a) F. Neese, *Wiley Interdiscip. Rev.: Comput. Mol. Sci.*, 2018, **8**, e1327; (b) F. Neese, *Wiley Interdiscip. Rev.: Comput. Mol. Sci.*, 2022, **12**, e1606.